https://doi.org/10.5194/egusphere-2025-6437
Preprint. Discussion started: 14 January 2026

Uncertainty of Antarctic sea ice concentration using passive microwave retrievals in the marginal ice zone

Marta Stentella[1,2,3], Ghislain Picard[1], Petra Heil[2,4], Jacqueline Boutin[5], Emmanuel Dinnat[6], and Stuart Corney[2,3]

[1]Institut des Géosciences de l'Environnement (IGE),Université Grenoble Alpes, Grenoble, France
[2]Australian Antarctic Program Partnership (AAPP), Hobart, Australia
[3]Institute for Marine and Antarctic Studies (IMAS), University of Tasmania, Hobart, Australia
[4]British Antarctic Survey (BAS), Cambridge, UK
[5]LOCEAN, Sorbonne Université, CNRS, IRD, MNHN, Laboratoire d'Océanographie et du Climat: Expérimentations et Approches Numériques, LOCEAN/IPSL, 75005 Paris, France
[6]NASA Goddard Space Flight Center, Greenbelt, MD, USA

Correspondence: Marta Stentella (marta.stentella@univ-grenoble-alpes.fr)

Abstract. Antarctic sea ice has experienced an unprecedented decline in the past decade (2016-2025). Changes in sea ice concentration (SIC) and derived sea ice extent have been monitored using microwave radiometers since the late 1970s, providing information about the polar response to global climate change, hence making SIC an invaluable variable for numerical models. However, in the highly dynamic Marginal Ice Zone (MIZ), the region in between the pack ice and the open ocean, physical properties undergo intense variability, which may impact the accuracy of the SIC products retrieved from brightness temperature measurements. For the purpose of this study, the MIZ is defined as the area with SIC between 15% and 80%. We simulate the variations of brightness temperature due to changes in the physical parameters describing the sea ice, the snow, and the ocean with the Snow Microwave Radiative Transfer Model (SMRT) and the Passive and Active Reference Microwave to Infrared Ocean model (PARMIO) for a range of prescribed SIC. We then apply the core of the Bootstrap SIC algorithm on the simulated brightness temperatures and compare the retrieved and prescribed SIC, yielding the SIC error. This allows us to assess the impact of changes on the SIC retrieval by means of numerical radiative transfer simulations. Our work identifies the key parameters leading to high uncertainty in the retrieval: in the snowpack, the liquid water content and snow grain size cause SIC uncertainties of 5 - 10% in the warm conditions MIZ. In the cold season, the most influential factor is the presence of thin ice, inducing errors up to 30%. Ocean roughness caused by the high-wind conditions affects both warm and cold seasons and gives rise to biases up to 15% on the lower SIC MIZ boundary. However, other snowpack parameters that were expected to modify the SIC results, such as the salinity or temperature, showed a negligible impact in the tested range. We found that the core of the Bootstrap algorithm is largely robust to the variations in the snowpack, with no parameter introducing errors greater than 10% across the MIZ SIC range. In contrast, ocean surface roughness due to wind speed and the presence of thin ice in the pixel are the variables leading to the greatest uncertainties, suggesting they are the primary targets to achieve more accurate SIC retrievals.

https://doi.org/10.5194/egusphere-2025-6437
Preprint. Discussion started: 14 January 2026

1 Introduction

The Marginal Ice Zone (MIZ) – the region that separates the pack ice from the open ocean – is a highly dynamic environment featuring continuous interaction between the ocean and the atmosphere (Morison and McPhee, 2001; Bennetts et al., 2022; Dumont, 2022; Vichi, 2022). These exchanges have ongoing impact on the physical structure of the sea ice and the characteristics of the snowpack on top of it (Massom et al., 2001). Physical drivers causing shifts in properties such as temperature, moisture content, or salinity within the snow–sea ice system, or wind speed in the atmosphere, lead to variations in the emissivity of the sea ice, atmosphere and ocean components (Macelloni et al., 2001; Meissner and Wentz, 2002; Mathew et al., 2009; Willmes et al., 2014)). Understanding of the drivers of the interactions between the sea ice, the ocean, and the atmosphere is essential to explain the factors that contribute to the decline of sea ice extent, including the unprecedented minimum recorded in the Southern Ocean in summer 2023 (Maksym, 2019; Purich and Doddridge, 2023).

The sea ice concentration (SIC) is the fraction of the ocean surface covered by sea ice in a pixel (Comiso, 2009), that is the spatial footprint of the sensor acquiring the measurement. Satellite observations are exploited to retrieve SIC through the brightness temperature (T_B) measured by microwave radiometers in frequencies commonly used in sea ice analysis, between $19\,\mathrm{GHz}$ and $89\,\mathrm{GHz}$, in the vertical (V) and horizontal (H) polarisation (Cavalieri et al., 1984; Swift et al., 1985; Comiso, 1985). Passive microwave (PM) observations are the basic means of investigation to study snow metamorphisms, changes in the physical properties of sea ice, or the ocean surface because they provide synoptic and continuous observations not available otherwise (Parkinson and Cavalieri, 2008; Comiso et al., 2017a, b).

The combination of brightness temperature observations at different frequencies or polarisations constitutes a signature that differs across surface types (Comiso et al., 1997). In the case of sea ice, it is dependent on the physical properties of the ice and snow cover. In Antarctica, not only the sea ice changes significantly with time and region, but also the snow on top of it. Snow on sea ice undergoes high variability due to redistribution caused by frequent strong winds, seawater flooding, salinity variations and snow ice formation from sea ice overload, and daily melt-thaw cycles. All these processes largely affect the surface and internal properties of the snow, which in turn leads to wide variations in T_B (Massom et al., 2001; Wang et al., 2024).

Understanding the impact of the varying properties of snow and ice on the retrieved SIC, in a rigorous and quantifiable way, remains a challenge in the Southern Ocean (Vichi, 2022), especially in the MIZ (Worby, 2004a), where the increasing contribution of the ocean to the pixel signal (due to low SIC), introduces further T_B signature variations alongside the processes of formation and development of sea ice (Matsumura and Ohshima, 2015; Paul et al., 2021).

This study evaluates errors in the SIC retrieval induced by changes in the physical properties of the snow–sea ice–ocean system. To understand the drivers of the PM signature variability, we perform a sensitivity analysis on these properties through a forward-modelling approach. We employ a technique based on the Bootstrap algorithm (Comiso, 1986) to compute the SIC from model outputs of each sensitivity experiment and compare the results against a reference simulation, treated as the true SIC. Thus, we evaluate the uncertainty introduced by each parameter on the retrieved SIC. We constrain the area of interest to the low-concentration MIZ, whose boundaries are considered between 15 and 80% SIC (Vichi, 2022). We use a combination of two state-of-the-art radiative transfer models to simulate the passive microwave observations of the ocean and sea ice components of the MIZ. These tools allow the simulation of a mixed pixel; representation of the MIZ configuration during the warm and cold seasons. The modelling of the sea ice is performed with the Snow Microwave Radiative Transfer Model (SMRT) (Picard et al., 2018), representing the radiative transfer in a multilayer snowpack, sea ice, underlying ocean and overlying atmosphere. The ocean is modelled with the Passive and Active Reference Microwave to Infrared Ocean (PARMIO) (Dinnat et al., 2023), used to simulate the emissivity of the ocean, overlaid by the atmosphere.

The paper is structured as follows: Sect. 2 provides the background on passive microwave SIC retrieval. Sections 3.1 and 3.2 describe the cryospheric and ocean components, respectively, for the mixed pixel simulation. The observations used to support the forward modelling approach are presented in Sect. 3.3. The model parametrisation is adopted to analyse the variability of the snow-covered sea ice signature in Sect. 3.4 and the algorithm for the sensitivity analysis of the ocean and sea ice parameters on SIC simulations is in Sect. 3.5. Results are presented in Sect. 4, first addressing the simulated observational variability and then the SIC sensitivity analysis. Finally, Sect. 5 discusses the findings, their limitations, and future perspectives.

2 Background

Numerous SIC retrieval algorithms rely on the contrast of microwave emission between the sea ice (high emission) and ocean (low emission) (Comiso et al., 1984; Steffen and Schweiger, 1991; Comiso, 1985; Markus and Cavalieri, 2000). They assume linear mixing, which means that the T_B observed over a mixed pixel is the sum of the T_B over its ocean and sea ice components weighted by their respective proportions (Comiso and Sullivan, 1986; Comiso, 2012; Ivanova et al., 2015; Comiso et al., 2017b; Meier and Stewart, 2020). These methods usually evaluate the linear relationship in a two-dimensional space defined by two microwave channels, a channel being the T_B at a given frequency and polarisation, hereafter denoted by its frequency in GHz followed by its polarisation (e.g., 19V). The most commonly used in sea ice studies are the 37V–37H or the 19V–37V, with the latter combination preferred in the Antarctic MIZ (Comiso and Sullivan, 1986; Ivanova et al., 2015; Meier and Stewart, 2020).

The Bootstrap algorithm (Comiso, 1986) exploits the fact that T_B for an observation P is the linear combination of the pure ocean T_B and pure sea ice T_B to compute SIC:

$$T_B(P) = T_I C_I + T_O(1 - C_I) \tag{1}$$

where C_I is the sea ice concentration, T_B is the observed brightness temperature, T_I is the brightness temperature of sea ice, and T_O is the brightness temperature of the ocean (Swift et al., 1985; Comiso, 1985).

The observed T_B over pixels with 100% ocean and 100% sea ice tend to appear as two very distinct clusters when represented in 19V–37V channel space (Swift et al., 1985; Comiso, 1985). The representative brightness temperature of the pure ice and ocean clusters define the tie points T_I and T_O in Eq. 1, respectively, for sea ice and ocean. Through the sea ice tie point (T_I), passes a line with a slope determined by daily linear regression of the 100% SIC cluster. Variations along this line result from modifications of sea ice and snowpack properties. Data points distributed around the ocean tie points represent 100% open water with different surface states. The tie points and the 100% SIC line are adjusted daily to account for the variability that depends on season and the meteorological conditions (Comiso, 2013). The T_B signatures in between these tie points belong to pixels with different SIC values (Eq. 1). However, different snow and ice characteristics lead to different T_B signatures also when considered in the same concentration, introducing a non-unique relationship between T_B and SIC.

3 Methods and Data

3.1 Cryospheric brightness temperature simulation

3.1.1 Snow and thick first-year sea ice simulation

We employ the SMRT model (Picard et al., 2018) to simulate the snow-covered sea ice system. The output is the T_B at the 19V and 37V channels for a pixel fully covered by sea ice. The input to the model describes a stack of horizontal layers and the selected theoretical framework to compute the electromagnetic interaction within the layers. The final configuration consists of a top one-layer atmospheric layer, a surface windpacked layer, an underlying depth hoar layer and two superimposed sea ice layers. The windpack here refers to a wind slab characterised by small grain size, while the depth hoar, usually forming during the cold season due to the temperature gradient in the snowpack deriving from the difference between that of the sea ice underneath and that of the atmosphere (Akitaya, 1974), is characterised by larger grains. To describe the low-concentration MIZ, we include first-year sea ice: a thinner, colder upper layer representative of the transitional conditions between the snowpack and the ice, and a thicker lower layer in contact with the ocean.

The overlying layer is a simple bulk atmosphere (`simple_atmosphere` in SMRT) where we prescribe angle-dependent emission in the upward (atmosphere to sensor) and downward (atmosphere to Earth to sensor) directions for each frequency channel as well as an input value for the atmospheric transmittance. These parameters are taken from the PARMIO output look-up tables and are thus consistent with those used in the ocean simulations to ensure coherence between the modelled sea ice and ocean systems.

The microstructure model used for the snow layers is the `unified_scaled_exponential` (Picard et al., 2022) which takes the microwave grain size l_{MW} as input (Picard et al., 2022). We compute l_{MW} as the product of the polydispersity and the Porod length. The microwave polydispersity value (Picard et al., 2022) is set to `0.7` for the windpack and `1.5` for the depth hoar. The Porod length is computed as:

$$l_p = \frac{4(1-\rho_{\text{snow}}/\rho_{\text{ice}})}{\text{SSA}\cdot\rho_{\text{ice}}} \tag{2}$$

where the SSA (the specific surface area of snow) is obtained from the snow optical radius in Table 1. The ice permittivity model is obtained by mixing the saline water permittivity at each frequency through the formulation by Meissner and Wentz (Meissner and Wentz, 2004), and the pure ice permittivity through the Matzler formula (Mätzler, 2006), using the Polder van Santen (pvs) formula (Polder and Van Santeen, 1946).

https://doi.org/10.5194/egusphere-2025-6437
Preprint. Discussion started: 14 January 2026

Both layers of sea ice use the type "first-year ice" defined in SMRT. Their thicknesses are of the order of 5 cm and 1 m for the thin and thick layer, respectively. The microstructure model is described with the hard spheres without stickiness (Tsang et al., 1985; Macelloni et al., 2001; Picard et al., 2014).

The calculation of the scattering and absorption coefficients is performed using the improved Born approximation (IBA). The radiative transfer equation is then solved with the discrete ordinate and eigenvalue method (DORT), with 128 streams.

3.1.2 Thin ice simulation

Thin ice is modelled as a single layer of type "first-year sea ice" and the two main parameters are the thickness of 0.05 m and the salinity of 13 PSU. The microstructure is modelled with the sticky hard sphere as in the thick sea ice simulations.

3.2 Ocean brightness temperature simulation

We use PARMIO model (Dinnat et al., 2023), to simulate the ocean T_B at 19 GHz and 37 GHz. PARMIO models the emissivity of a flat ocean using Fresnel coefficients driven by the seawater permittivity model from Meissner and Wentz (Meissner and Wentz, 2004). Ocean surface waves represented through the Durden-Vesecky wave spectrum (Durden and Vesecky, 1985) multiplied by a factor 1.25 contribute to the T_B perturbation and are simulated with a two-scale model. The scattering of small waves, which are less than 4 times the radiometer wavelength, is calculated with the Small Perturbation Method (SPM) while the scattering of the large waves is calculated with the geometrical optics (GO) model. A further contribution comes from the foam-covered layer where the foam fraction follows the Monahan description (Monahan and Lu, 1990) and the foam emissivity, the Yin formulation (Yin et al., 2016). The foam fraction varies as a function of the wind speed. The reference ocean output incorporates both the foam impact and the atmospheric contribution as included in the PARMIO model, for the benchmark case we choose a wind speed of 15 ms^{-1}. The warm and cold season reference configurations differ for the sea water temperature: 0 °C and -1.9 °C respectively.

3.3 AMSR-2 passive microwave observations

Advanced Microwave Scanning Radiometer2 (AMSR2) data are extracted from the unified collection of AMSR sensors, NSIDC DAAC Advanced Microwave Scanning Radiometer Unified AMSR-U (Meier et al., 2017). AMSR-2, aboard the Japanese satellite Global Change Observation Mission 1^{st}-Water, "SHIZUKU" (GCOM-W1), provided observations from July 2012. These products include observed T_B and estimated SIC for both ascending and descending orbits. We use T_B at 19 GHz and 37 GHz in vertical polarisation under an angle of incidence of 55° and on a common grid of $12.5\times12.5\ \mathrm{km}^2$ resolution.

We applied a mask to the dataset to select the sea ice area and a limited portion of adjacent open ocean. The mask was created using the sea ice concentration (>15%) corresponding to the date under analysis for the warm and cold seasons, and extending it 30 km into the ocean.

Table 1. Physical properties of the snowpack input in the SMRT model for warm and cold seasons. 'Value REF'is the reference value most representative of seasonal observations. The 'Min'and 'Max'columns define the parameter range used in the sensitivity analysis.

Parameter	**Warm season**			**Cold season**		
	Value REF	**Min**	**Max**	**Value REF**	**Min**	**Max**
WINDPACK						
Thickness_SP (m)	0.1	0	0.2	0.2	0	0.3
Density_SP ($\mathrm{kg\,m^{-3}}$)	370	200	450	350	200	450
Temperature_SP (K)	273.15	263.15	273.15	260.15	253.15	273.15
Radius_SP (μm)	100	50	400	170	100	200
Salinity_SP (PSU)	3	0	10	5	0	12
Fraction_volume_water_SP	0	0	0.2	0	0	0.2
DEPTH HOAR						
Thickness_DH (m)	0.03	0	0.1	0.025	0	0.2
Density_DH ($\mathrm{kg\,m^{-3}}$)	300	200	450	230	200	350
Temperature_DH (K)	273.15	263.15	273.15	270.15	253.15	273.15
Radius_DH (μm)	300	50	500	250	200	500
Salinity_DH (PSU)	5	0	8	7	0	8
Fraction_volume_water_DH	0.025	0	0.2	0.02	0	0.2
SEA ICE 1						
Thickness_SI_1 (m)	0.05	0	0.1	0.07	0	0.1
Density_SI_1 ($\mathrm{kg\,m^{-3}}$)	915	–	–	915	–	–
Temperature_SI_1 (K)	269.15	269.15	271.15	269.00	268.15	270.15
Radius_SI_1 (μm)	2	–	–	2	–	–
Salinity_SI_1 (PSU)	10	7	12	12	7	15
SEA ICE 2						
Thickness_SI_2 (m)	0.95	–	–	1	–	–
Density_SI_2 ($\mathrm{kg\,m^{-3}}$)	915	–	–	915	–	–
Temperature_SI_2 (K)	271.15	–	–	271.15	–	–
Radius_SI_2 (μm)	2	–	–	2	–	–
Salinity_SI_2 (PSU)	8	–	–	8	–	–

3.4 Microwave brightness temperature modelling across the marginal ice zone: variability of sea ice observations

The first part of this work analyses the spread observed in AMSR2 brightness temperature within the 19V–37V space. We simulate a mixed pixel as the linear combination of the T_B of the snow covered sea ice, output of the SMRT (Picard et al., 2018) model (Sect. 3.1.1) and the T_B of the ocean, obtained using PARMIO (Dinnat et al., 2023) (Sect. 3.2).

First, we select individual days of AMSR2 observations within the warm and the cold season to generate and calibrate the seasonal tie points through forward modelling. These tie points are the optimal representative for T_O and T_I in Eq. 1, for the selected date. The initial selection of the physical parameters is informed by literature (Cox and Weeks, 1974; Brucker et al., 2010; Petrich and Eicken, 2017; Soriot et al., 2022; Lawrence et al., 2024). These parameters are subsequently adjusted to match the observations so that the simulated T_B in the 19V and 37V channels visually overlaps with the 100% sea ice and ocean clusters of AMSR2 observations. The reference model configuration chosen for the sea ice is described in Table 1 and Sect. 3.1.1, and for the ocean in Sect. 3.2.

In the second step, we iteratively vary each parameter across the range defined by the minimum and the maximum values in Table 1, while keeping the others constant at the reference value (Table 1).

Finally, in the third step, the linear combination of the derived T_O and T_I at 10% interval (Eq. 1), yields mixed pixel simulations that capture the variability observed in the daily AMSR2 MIZ observations for different ice types.

3.5 Sea ice concentration sensitivity analysis

3.5.1 SIC sensitivity to snow and sea ice parameters

The sensitivity analysis algorithm for each snow and sea ice physical parameter leverages the tie points from the reference model simulation (Sect. 3.1; 3.2) determined in Sect. 3.4 and is implemented as follows:

1. Use reference tie points calibrated on the 19V–37V observations as in Sect. 3.4: SMRT output for 100% SIC (point A in Fig. 1), parametrised as in Sect. 3.1.1 and PARMIO output for 100% open ocean (point O in Fig. 1), parametrised as in in Sect. 3.2.

2. For each parameter variation across its Table 1 range, iteratively run both models and linearly combine the resulting T_B values (Eq. 1) at 15%, 30%, 50%, and 80% SIC to determine the modelled MIZ mixed pixel signature (points P, Fig. 1) for different ice-types as described in Sect. 3.4.

3. Determine the slope of the 100% SIC line (line A in Fig. 1). We use the least-square linear regression in the two-channel space of the 100% SIC T_B cluster values for the analysed date.

4. Determine the intercept with the 100% SIC line (point I in Fig. 1). To do so, we compute the equation for the line through the modelled observation P and the ocean tie point O.

5. Retrieve the SIC corresponding to each modified configuration via geometric interpolation (Comiso, 1985, 2013), computing the ratio :

$$\mathrm{SIC} = \frac{|\overline{OP}|}{|\overline{OI}|} = \left(\frac{T_P - T_O}{T_I - T_O}\right), \tag{3}$$

   where points O, P and I are determined respectively in steps 1,2 and 4.

6. Calculate the difference between the retrieved and prescribed SIC for each parameter value.

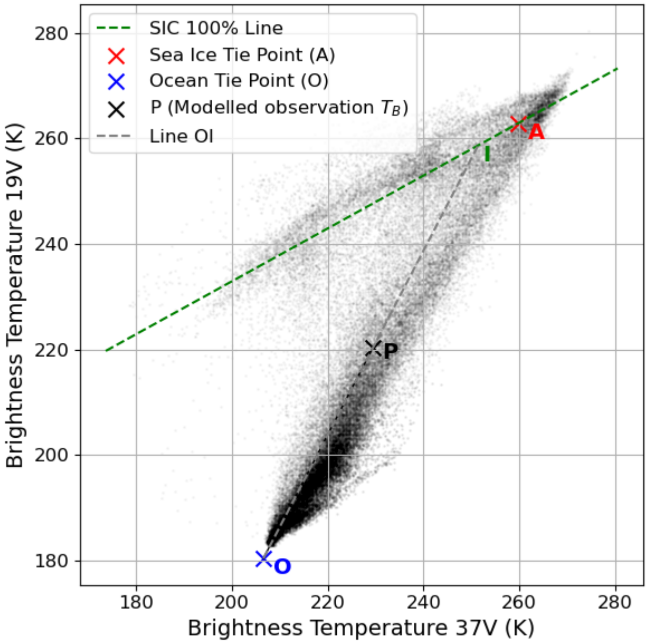

Figure 1. SIC retrieval algorithm description. Brightness temperature at 19V versus 37V from AMSR2 observations (black dots). A and O are, respectively, the tie points for 100% SIC sea ice (SMRT output) and open ocean (PARMIO output). The top green line through Line A (green dashed line) is the linear regression of the 100% SIC cluster. Point P is an observational modelled point at 50% SIC (output of SMRT warm season reference snowpack with dry depth hoar layer). Line P (dashed grey line) through the ocean tie point intercepts line A in I.

3.5.2 SIC sensitivity to thin ice presence

The sensitivity analysis for the thin ice component quantifies the impact of different thin ice fractions on total SIC. We compare the T_B of the 100% SIC reference tie point A corresponding to the snow-covered sea ice, computed in section 3.5.1, with the T_B computed when thin ice constitutes a fraction of 0, 0.1, 0.3, 0.5, 0.8 and 1 of the total first-year ice. This analysis is repeated for SIC values of point 2 in Sect. 3.5.1 , and for multiple salinity values across the range specified in Table 2. In addition, a range of thicknesses between 1 cm and 7 cm has been tested while holding the reference parametrisation as in Table 2.

https://doi.org/10.5194/egusphere-2025-6437
Preprint. Discussion started: 14 January 2026

Table 2. Physical and microstructural properties of thin first-year sea ice used in the SMRT model.

Parameter	Value REF	Min	Max
THIN SEA ICE			
Thickness (m)	0.05	0.03	0.07
Density (kgm^{-3})	915	–	–
Temperature (K)	271.15	–	–
Radius (μm)	2	–	–
Salinity (PSU)	13	10	20
Microstructure model	Sticky hard spheres	–	–
Stickiness	100	–	–
Water substrate	True	–	–

3.5.3 SIC sensitivity to ocean surface roughness

The sensitivity analysis for the ocean component assesses the impact of surface roughness variations on SIC. To do so, we use the model setup as described in Sect. 3.2 and we modulate the wind speed in 1 ms^{-1} increments over a range from 2.5 ms^{-1} to 30 ms^{-1}. The SIC sensitivity analysis is analogous to the method described in Sect. 3.5.1 with one modification: in step 2, we vary the ocean physical parameter (i.e., the wind speed) while keeping the reference sea ice tie point A. Each new combination (37V–19V) of ocean T_B resulting from a variation in the wind speed (relative to the reference of 15 ms^{-1}), is considered an observational point P, to which steps 3 to 6 are applied.

4 Results

4.1 Sensitivity analysis in warm and cold season

During the warm season, the scatter of the observations around the line connecting the tie points (Fig. 2) is captured through the range of values assumed by the parameters in Table 1. Figure 2 shows that the liquid water content (LWC) exhibits the greatest variability both in the windpacked layer (Fig. 2a) and in the depth hoar (Fig. 2g), followed by the thickness (Fig. 2h) and the optical radius (Fig. 2e and k). Density, temperature and salinity changes show negligible impact on the T_B across the two snowpack layers (Fig. 2d, f, j and l). On the other hand, thickness, temperature and salinity in the topmost layer of sea ice, show larger changes in T_B when considering the extremes of the tested range (Fig. 2m, n and o). The deeper sea ice layer does not affect the T_B signature (result not shown).

Figure 3 shows that, in the cold season, parameter changes have a more contained impact compared to the warm season (Fig. 2). This is evident in the snowpack layer (Fig. 3a to f). The T_B signature shows highest sensitivity to LWC, optical radius and thickness; however, unlike the warm condition, this occurs predominantly in the depth hoar layer (Fig. 3g to l).

https://doi.org/10.5194/egusphere-2025-6437
Preprint. Discussion started: 14 January 2026

Figure 4 illustrates the impact of the primary driver of the ocean sensitivity: the wind speed. Although wind speeds up to $30\,\mathrm{ms}^{-1}$ are considered in the simulations, the spread of the observations is not fully captured by the model chain. However, a significant portion of the observed cluster around the ocean tie point and its trend is reproduced in the output T_{Bs} at 0% SIC (Fig. 4).

Thin ice T_B (Fig. 5a) exhibits a wide spread exceeding $20\,\mathrm{K}$, depending on the salinity. As shown in Fig. 5a, the thin ice T_B signature is closer to the sea ice tie point at low salinity values. In contrast, at high salinities characteristic of the initial stages of sea ice growth, the T_B signature shifts towards the ocean reference point.

4.2 Sea ice concentration uncertainty

In line with the sensitivity analysis (Sect. 4.1), the highest impact on the SIC retrieval bias (in %) is primarily attributed to the LWC and the optical radius in the snowpack layers (Fig. 6d, e), with the windpacked layer being the dominant source of uncertainty (Fig. 6). While for SIC values below 50%, LWC and optical radius induce errors smaller than 5%; when considering SIC up to 80%, the resulting uncertainty increases, but remains below 10% (Fig. 6d and Fig. 6e). In the depth hoar layer, the thickness, optical radius, and LWC all contribute similarly, each causing an error within 5%. The thickness and temperature of the uppermost sea ice layer (Fig. 6a, b) impact the simulated SIC at the extremes of their variation range; for instance, when the layer is absent (null thickness).

Figure 7 illustrates that SIC retrieval is highly sensitive to changes in ocean surface roughness when the ocean dominates the pixel T_B signature. Towards the lower limit of 15% SIC in the MIZ, errors can exceed 10% under strong wind conditions, up to $30\,\mathrm{ms}^{-1}$.

Figure 8d shows that the liquid water content remains the major driver in the cold season as well. When it exceeds 10% in any snowpack layer, the uncertainty on the higher SIC MIZ boundary (80%) is still limited to less than 5%. Slightly wet snow in the top layer leads to SIC underestimation (Fig. 8d blue crosses), but high liquid water content (20%) in the depth hoar (Fig. 8d orange squares), causes overestimation. We observe lower uncertainties affecting the simulated SIC in the cold season compared to the warm season (Fig. 6 versus Fig. 8). All the windpack parameters, for instance, induce negligible errors in the retrieved SIC. Depth hoar thickness and radius have the next most significant influence, yielding uncertainties that remain constrained to less than 5% across the SIC values (Fig. 8a,e).

As shown in Sect. 4.1, T_B signature variations in thin ice exceed those of the snowpack, yielding the presence of thin ice to induce substantial biases in the retrieved SIC. Inclusion of thin ice with low salinity of approximately 10 PSU results in a SIC underestimation limited to 10%. However, at higher salinity values and higher thin ice fraction within a pixel, SIC retrieval errors range between 10% and 30% (Fig. 5b).

5 Discussion

In this work, we have considered the variations in physical properties of the ocean surface, the snowpack and the first-year sea ice, to assess their impact on the radiometric signal. Our analysis identified key variables (e.g., liquid water content, optical

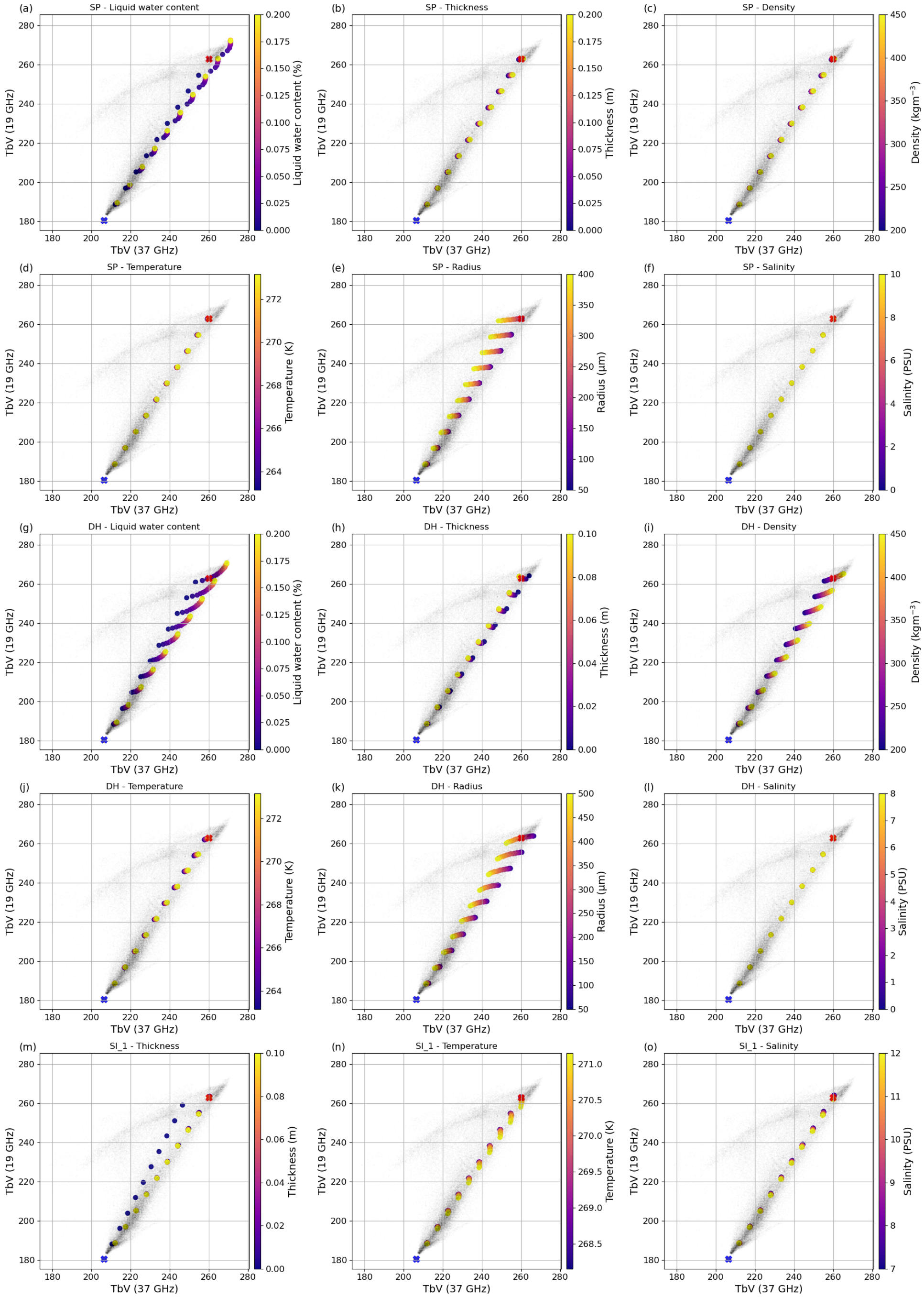

Figure 2. Brightness temperature signature in the 19V–37V space corresponding to variations in the physical properties of sea ice and snowpack layers, as obtained with the three-steps method described in Sect. 3.4. The MIZ T_B observations from AMSR-2 (black dots) represent warm conditions (2015-01-20). Each subplot examines a single parameter for a specific layer: windpack (SP), depth hoar (DH), or top layer of first-year sea ice (SI_1). Data points for 100% SIC (red cross) and open ocean (blue cross) serve as reference tie points. Each data point is coloured by parameter value and it derives from a linear SIC combination (each 10%) of modelled variations from the reference configuration.

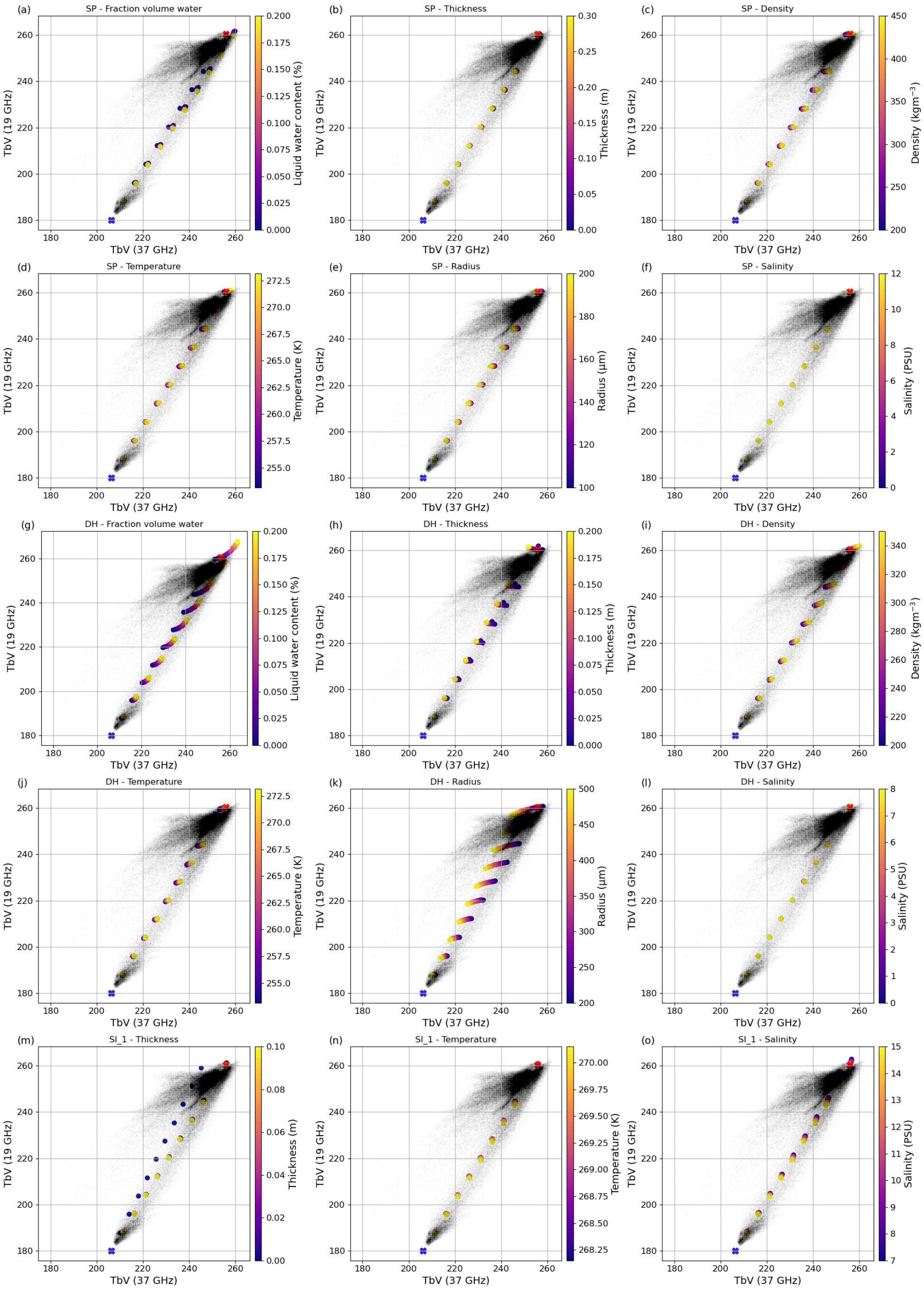

Figure 3. Same as figure 2 for cold season conditions (2015-06-20).

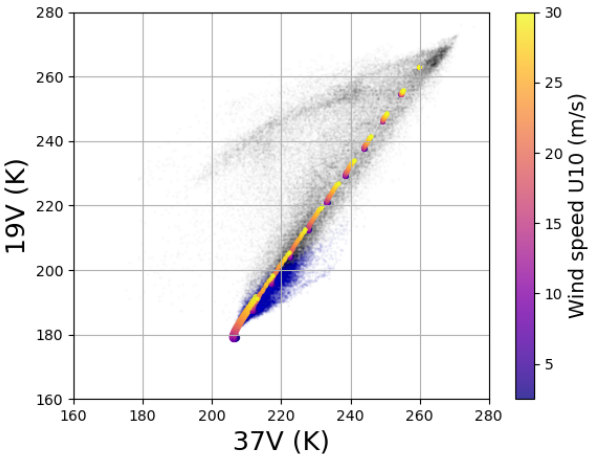

Figure 4. Brightness temperature signature in the 19V–37V space corresponding to wind-induced ocean surface property variations. The MIZ T_B observations (black dots) and open ocean observations (blue dots) from AMSR-2 correspond to warm conditions (2015-01-20). Both the observation clusters are masked as described in section 3.3. Each data point is coloured by wind speed value and it derives from a SIC linear combinations.

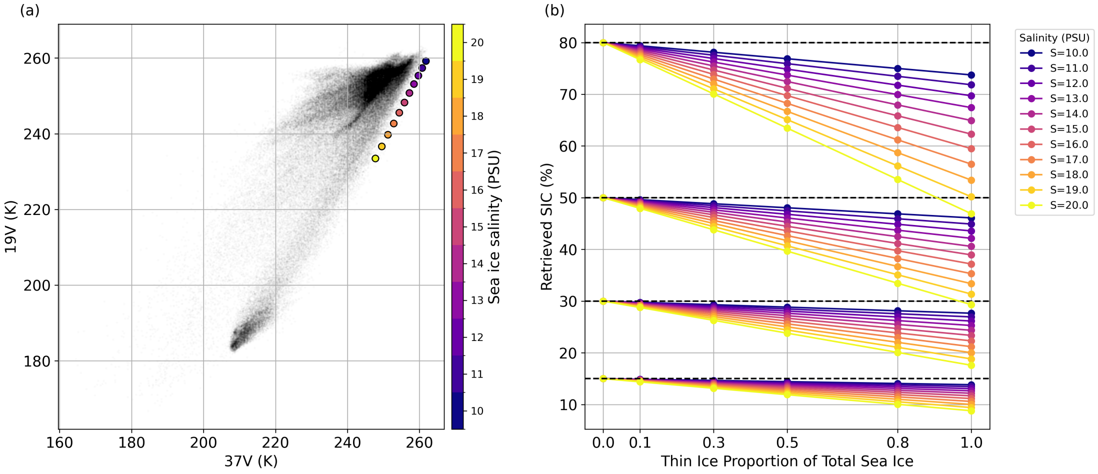

Figure 5. (a) Brightness temperature signature in the 19V–37V space corresponding to variations in the salinity of thin ice, as obtained with the method described in Sect. 3.5.2. The MIZ T_B observations from AMSR-2 (black dots) represent cold season conditions (2015-06-20). Each data point is coloured by salinity value, and it's modelled for 100% SIC. (b) Retrieved SIC when varying proportions of thin ice are included in the thick first-year sea ice signature. Different thin ice salinity values are colour-coded and the true SIC (15%, 30%, 50%, 80%) is marked by horizontal lines.

https://doi.org/10.5194/egusphere-2025-6437
Preprint. Discussion started: 14 January 2026

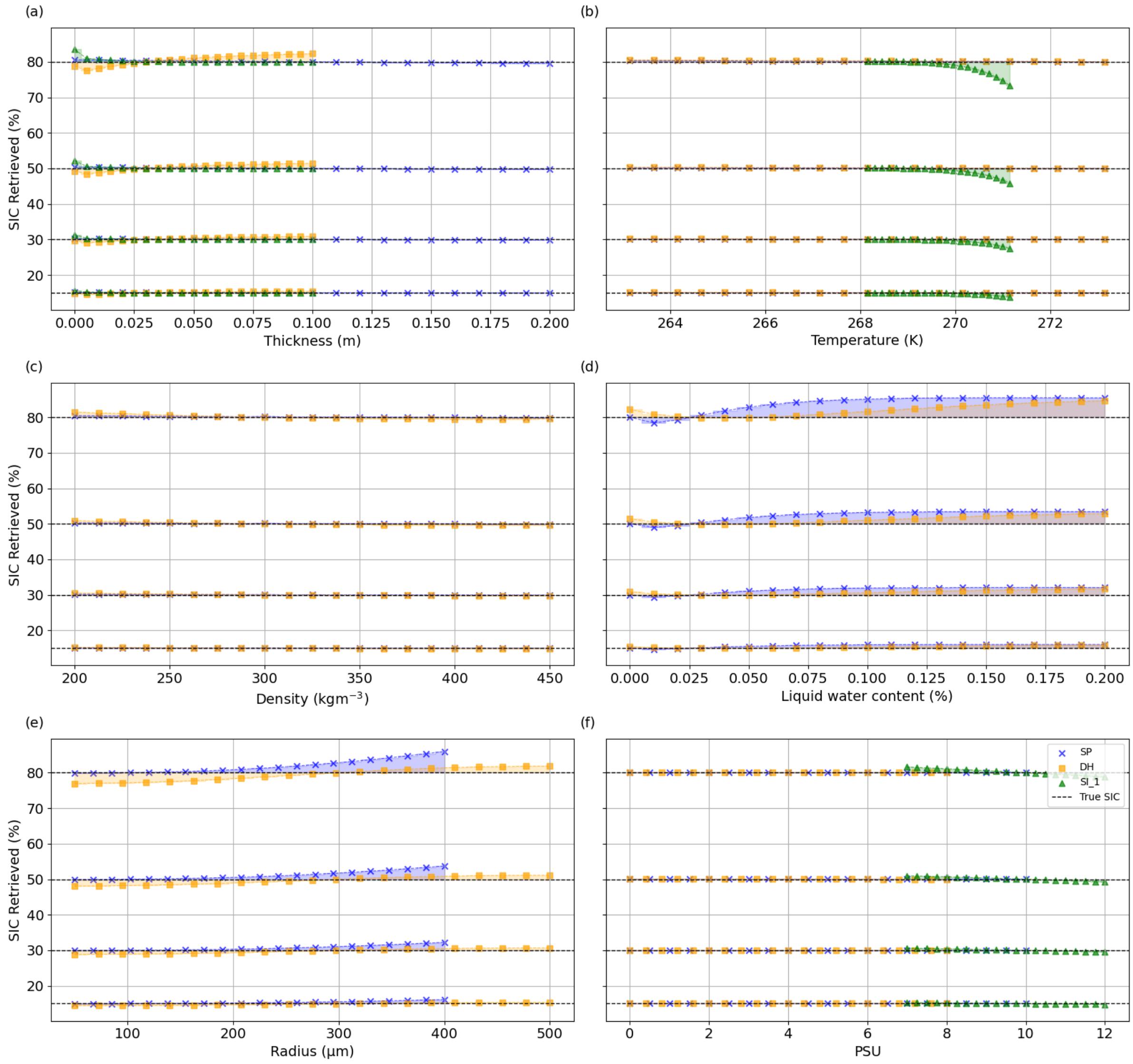

Figure 6. Warm season (2015-01-20). SIC retrieved for individual parameter variations from the reference snowpack and sea ice. True SIC values (15%, 30%, 50%, 80%) are represented by horizontal lines. For each layer –windpack (SP, blue crosses), depth hoar (DH, orange squares), top first-year sea ice (SI_1, green triangles)– the retrieved SIC is plotted for regularly spaced values within the range defined in Table 1.

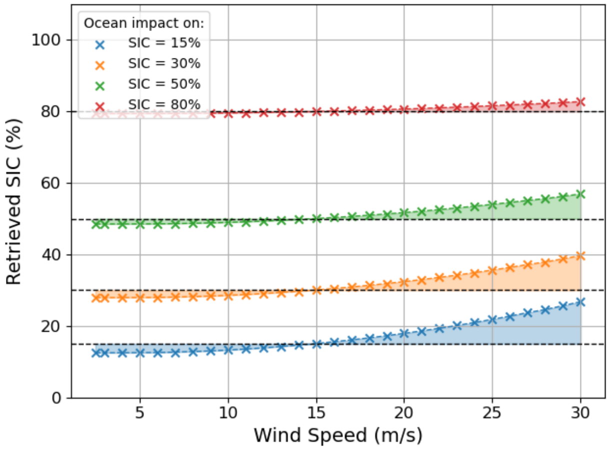

Figure 7. Warm season (2015-01-20). SIC retrieved for wind speed variation from the reference ocean parametrisation ($15\,\mathrm{ms}^{-1}$). True SIC values (15%, 30%, 50%, 80%) are represented with horizontal lines. Data points are coloured by SIC and shown for increasing wind speeds from 2 to $30\,\mathrm{ms}^{-1}$.

radius and thickness for the snow-covered sea ice, wind speed for the ocean and highly saline thin ice) to which the T_B signature is more sensitive, leading therefore, to greater errors in the SIC simulated through the algorithm employed (Sect. 4.2). These simulations allow to reproduce the T_B changes in the 37V–19V space, especially in the warm season (Fig. 2), where the range of parameters, such as the liquid water content or the snow optical radius, shows a broader spread. The snowpack in the warm season accounts for the greatest variation in the T_B signature, which is therefore reflected in a greater uncertainty in the retrieved SIC (Fig. 6; Fig. 8). In line with existing literature, the algorithm provides higher accuracy to snow types in the winter season compared to the summer season (Meier and Notz, 2010; Ivanova et al., 2015). In (Comiso, 2013), the error on the SIC is often limited to 3% during the cold season. On the other hand, during the melt season represented by our modelled warm configuration, the liquid water content leads to a higher imaginary part of the effective permittivity. This means higher absorption and therefore higher emissivity than in dry snow, when considering LWC exceeding 2%-3% (Comiso, 2013). The rise of this value leads to T_B saturation. This process, in Fig. 6d, introduces uncertainty in the real emissivity of snow and causes an overestimation of SIC.

During the cold season, the error caused by the cryospheric component is more limited compared to the warm season. This is due to a more constrained T_B variation around the modelled reference snowpack, also noticeable in the observations (Fig. 2 and 3). Deviations from the line through the tie points are therefore limited, resulting in lower biases in the SIC retrieval. On the other hand, the presence of thin ice produces uncertainties in the simulated SIC, significantly more influential than those from any other parameter in the warm season (Meier et al., 2017). A variation in the thin ice fraction included in the first-year sea ice, with salinity values between 15 and 20 PSU can account for errors 10-20% larger than those generated by the other snow and sea ice parameters (Fig. 5b). This sensitivity depends on the thin ice development stage, and therefore on its properties, particularly the salinity (Comiso, 2012, 2013), determining whether the T_B is closer to T_O or T_I, as observable in Fig. 5a.

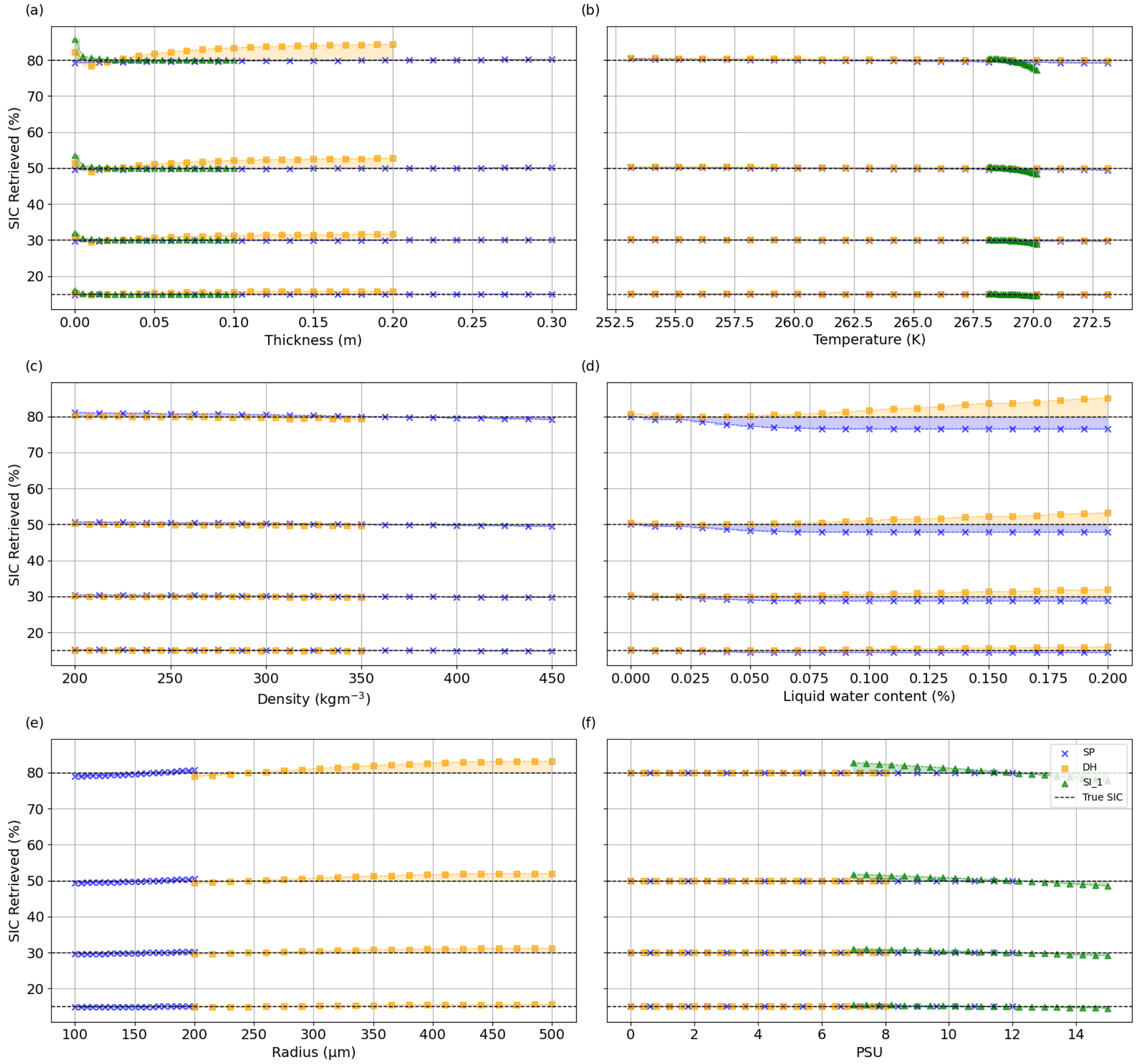

Figure 8. Same as figure 6 for cold season conditions (2015-06-20). The parameter range is defined in Table 1.

https://doi.org/10.5194/egusphere-2025-6437
Preprint. Discussion started: 14 January 2026

The impact of ocean surface variations is limited when approaching areas of consolidated ice (SIC >80%) (Fig. 7). However, when considering the ice edge (15-30%), the error in the SIC retrieved can be up to 10%-15%, which confirms the difficulty in determining the ice edge and in providing an accurate SIC estimation under rough ocean surface conditions (Worby, 2004b; Meier and Stroeve, 2008; Comiso, 2013). In addition, these results are limited by the reliability of the models, especially at high wind speeds. PARMIO achieves higher accuracy with wind speed up to $15\,\mathrm{ms}^{-1}$ where the bias in T_B corresponds to an underestimation within 5 K with respect to the observations. Nevertheless, Fig. 4 shows consistency between our simulated ocean T_B and the AMSR2 observations.

The errors on SIC caused by single parameters are found to agree with those documented in the literature (Ivanova et al., 2015; Comiso, 2009; Andersen et al., 2007). We confirmed larger uncertainties in the warm season, particularly due to increasing open water fractions in the pixel and the presence of liquid water associated with melt in the snowpack (Meier and Notz, 2010). On the other hand, the presence of thin ice is the main contributor to the bias in the retrieved SIC, especially in the cold season (Notz and Worster, 2009; Gough et al., 2012).

A first limitation of our modelling approach is that it assumes, as background observations for the forward modelling, a mask including the entirety of the circumpolar MIZ, thereby not accounting for regional-scale heterogeneity in the snow, ocean, and sea ice physical characteristics. Future development of this work should focus on a finer scale analysis to capture the physical changes reflected in the parameter range describing the system following intense weather events and ocean forcing. Variations in properties that could otherwise be concealed or averaged, preventing the actual estimation of SIC. In addition, while defining the slope of the 100% SIC line through linear regression as prescribed in the Bootstrap method (Fig. 1) is appropriate at the large scale, it could limit the accuracy of the results on a local scale.

Another limitation stems from the difficulty of capturing, in the T_B signature interpretation, the strong seasonality of the sea ice characteristics (Comiso et al., 2003). Key processes include snow accumulation and metamorphism leading to intense layering typical of the Antarctic continent (Massom et al., 2001; Nicolaus et al., 2009; Toyota et al., 2011), surface flooding or yet, dynamic emissivity profiles for the thin ice depending on its age and thickness (Comiso and Steffen, 2001; Notz and Worster, 2009). Nevertheless, these processes, together with atmospheric effects on T_B exert the largest influence mainly on the polarisation ratio (Cavalieri et al., 1984) which is not used in our method. We relied on 19 GHz and 37 GHz in the vertical channels and a simple one-layer atmosphere.

Finally, this analysis treats parameters independently: extensions of this work should consider potential simultaneous variations and their propagation on the SIC retrieval, providing further accuracy to its estimate in the MIZ.

6 Conclusions

This study set out to differentiate the relevant physical parameters characterising T_B changes that contribute to the variability in passive microwave information of the Southern MIZ, with the aim to infer the impact of different parametrisations on the SIC retrieval.

The response to the specific microwave parametrisation exhibits seasonality. We show that the dominant sources of uncertainty in the warm season are the liquid water content and the optical radius in the snowpack for high SIC in the MIZ. On the other hand, the ocean surface roughness is primarily responsible for biases at low concentrations of sea ice (15% - 30%).

The cold season shows a similar behaviour in the ocean T_B. However, the T_B signature of the snow-covered sea ice undergoes less variation than in the warm season, resulting in more accurate SIC retrievals. In contrast, during this season, thin ice ($< 0.1\,\mathrm{m}$) represents the most significant source of uncertainty.

Our results, derived from the application of a novel forward modelling approach to simulate mixed pixels, identify uncertainties and offer a context for their origin. We provide order-of-magnitude quantification of how variations in physical parameter ranges impact SIC inference across different sea ice concentrations in the MIZ. These modelled uncertainties are consistent with literature values derived from applying an operational SIC retrieval algorithm to observations. Importantly, we demonstrated improved sea ice concentration through the interpretation of the radiometric signal using the SMRT and PARMIO models. Applying this method to obtain accurate SIC estimates will deliver enhanced sea ice extent information, especially for regional studies.

Code and data availability. The sea ice and ocean configuration files and model outputs generated for this study are available at https://github.com/StentelMarta/Uncertainty_Antarctic_SIC_retrievals.git.

Author contributions. MS and GP designed the analysis method. PH and GP set the context and direction for this study. MS conducted the study. JB and ED participated in the discussion for the parametrisation of the PARMIO model. ED compared the brightness temperatures simulated with the PARMIO model configuration to AMSR2 observations. Allco-authors discussed and revised the manuscript.

Competing interests. One of the co-authors, PH, is a member of the editorial board of The Cryosphere.

Acknowledgements. This study is an outcome of the AUFRANDE project, which is co-funded by the European Union under the Marie Skłodowska-Curie Grant Agreement No 101081465 (AUFRANDE). Views and opinions expressed are however, those of the authors only and do not necessarily reflect those of the European Union or the Research Executive Agency. Neither the European Union nor the Research Executive Agency can be held responsible for them. MS and PH acknowledge award #501 of the International Space Science Institute. PH acknowledges support from the Australian Government as part of the Antarctic Science Collaboration Initiative (ASCI000002), and the Australian Government's Australian Antarctic Science Program grant 4625. During the early part of this study, PH was with the Australian Antarctic Division (AAD), Kingston, Australia, as well as on a Fellowship with the Swiss Federal Institute for Snow & Avalanche Research (SLF), Davos, Switzerland.

References

Akitaya, E.: Studies on depth hoar, Contributions from the Institute of Low Temperature Science, 26, 1–67, 1974.

Andersen, S., Tonboe, R., Kaleschke, L., Heygster, G., and Pedersen, L. T.: Intercomparison of passive microwave sea ice concentration retrievals over the high-concentration Arctic sea ice, Journal of Geophysical Research: Oceans, 112, 2006JC003 543, https://doi.org/10.1029/2006JC003543, 2007.

Bennetts, L. G., Bitz, C. M., Feltham, D. L., Kohout, A. L., and Meylan, M. H.: Marginal ice zone dynamics: future research perspectives and pathways, Philosophical Transactions of the Royal Society A: Mathematical, Physical and Engineering Sciences, 380, 20210 267, https://doi.org/10.1098/rsta.2021.0267, number: 2235, 2022.

Brucker, L., Picard, G., and Fily, M.: Snow grain-size profiles deduced from microwave snow emissivities in Antarctica, Journal of Glaciology, 56, 514–526, https://doi.org/10.3189/002214310792447806, number: 197, 2010.

Cavalieri, D. J., Gloersen, P., and Campbell, W. J.: Determination of sea ice parameters with the NIMBUS 7 SMMR, Journal of Geophysical Research: Atmospheres, 89, 5355–5369, https://doi.org/10.1029/JD089iD04p05355, 1984.

Comiso, J.: SSM/I Concentrations using the Bootstrap Algorithm, NASA RP-1380 (NASA Reference Publication 1380), 1985.

Comiso, J.: amsr-atbd-supp12-seaice, 2012, 2012.

Comiso, J., Cavalieri, D., and Markus, T.: Sea ice concentration, ice temperature, and snow depth using AMSR-E data, IEEE Transactions on Geoscience and Remote Sensing, 41, 243–252, https://doi.org/10.1109/TGRS.2002.808317, 2003.

Comiso, J. C.: Characteristics of Arctic winter sea ice from satellite multispectral microwave observations, Journal of Geophysical Research: Oceans, 91, 975–994, https://doi.org/10.1029/JC091iC01p00975, 1986.

Comiso, J. C.: Enhanced Sea Ice Concentrations and Ice Extents from AMSR-E Data, https://doi.org/10.11440/rssj.29.199, 2009.

Comiso, J. C.: Descriptions of GCOM-W1 AMSR2 Level 1R and Level 2 Algorithms JAXA, AMSR2 ATBD, 2013.

Comiso, J. C. and Steffen, K.: Studies of Antarctic sea ice concentrations from satellite data and their applications, Journal of Geophysical Research: Oceans, 106, 31 361–31 385, https://doi.org/10.1029/2001JC000823, 2001.

Comiso, J. C. and Sullivan, C. W.: Satellite microwave and in situ observations of the Weddell Sea ice cover and its marginal ice zone, Journal of Geophysical Research: Oceans, 91, 9663–9681, https://doi.org/10.1029/JC091iC08p09663, 1986.

Comiso, J. C., Ackley, S. F., and Gordon, A. L.: Antarctic sea ice microwave signatures and their correlation with in situ ice observations, Journal of Geophysical Research: Oceans, 89, 662–672, https://doi.org/10.1029/JC089iC01p00662, number: C1, 1984.

Comiso, J. C., Cavalieri, D. J., Parkinson, C. L., and Gloersen, P.: Passive microwave algorithms for sea ice concentration: A comparison of two techniques, Remote Sensing of Environment, 60, 357–384, https://doi.org/10.1016/S0034-4257(96)00220-9, 1997.

Comiso, J. C., Gersten, R. A., Stock, L. V., Turner, J., Perez, G. J., and Cho, K.: Positive Trend in the Antarctic Sea Ice Cover and Associated Changes in Surface Temperature, Journal of Climate, 30, 2251–2267, https://doi.org/10.1175/JCLI-D-16-0408.1, 2017a.

Comiso, J. C., Meier, W. N., and Gersten, R.: Variability and trends in the Arctic sea ice cover: Results from different techniques, Journal of Geophysical Research: Oceans, 122, 6883–6900, https://doi.org/10.1002/2017JC012768, 2017b.

Cox, G. F. N. and Weeks, W. F.: Salinity Variations in Sea Ice, Journal of Glaciology, 13, 109–120, https://doi.org/10.3189/S0022143000023418, 1974.

Dinnat, E., English, S., Prigent, C., Kilic, L., Anguelova, M., Newman, S., Meissner, T., Boutin, J., Stoffelen, A., Yueh, S., Johnson, B., Weng, F., and Jimenez, C.: PARMIO: A Reference Quality Model for Ocean Surface Emissivity and Backscatter from the Microwave to the Infrared, Bulletin of the American Meteorological Society, 104, E742–E748, https://doi.org/10.1175/BAMS-D-23-0023.1, 2023.

Dumont, D.: Marginal ice zone dynamics: history, definitions and research perspectives, Philosophical Transactions of the Royal Society A: Mathematical, Physical and Engineering Sciences, 380, 20210 253, https://doi.org/10.1098/rsta.2021.0253, number: 2235, 2022.

Durden, S. and Vesecky, J.: A physical radar cross-section model for a wind-driven sea with swell, IEEE Journal of Oceanic Engineering, 10, 445–451, https://doi.org/10.1109/JOE.1985.1145133, 1985.

Gough, A. J., Mahoney, A. R., Langhorne, P. J., Williams, M. J. M., and Haskell, T. G.: Sea ice salinity and structure: A winter time series of salinity and its distribution, Journal of Geophysical Research: Oceans, 117, 2011JC007 527, https://doi.org/10.1029/2011JC007527, 2012.

Ivanova, N., Pedersen, L. T., Tonboe, R. T., Kern, S., Heygster, G., Lavergne, T., Sørensen, A., Saldo, R., Dybkjær, G., Brucker, L., and Shokr, M.: Satellite passive microwave measurements of sea ice concentration: an optimal algorithm and challenges, https://doi.org/10.5194/tcd-9-1269-2015, 2015.

Lawrence, I. R., Ridout, A. L., Shepherd, A., and Tilling, R.: A Simulation of Snow on Antarctic Sea Ice Based on Satellite Data and Climate Reanalyses, Journal of Geophysical Research: Oceans, 129, e2022JC019 002, https://doi.org/10.1029/2022JC019002, 2024.

Macelloni, G., Paloscia, S., Pampaloni, P., and Tedesco, M.: Microwave emission from dry snow: a comparison of experimental and model results, IEEE Transactions on Geoscience and Remote Sensing, 39, 2649–2656, https://doi.org/10.1109/36.974999, 2001.

Maksym, T.: Arctic and Antarctic Sea Ice Change: Contrasts, Commonalities, and Causes, Annual Review of Marine Science, 11, 187–213, https://doi.org/10.1146/annurev-marine-010816-060610, number: 1, 2019.

Markus, T. and Cavalieri, D.: An enhancement of the NASA Team sea ice algorithm, IEEE Transactions on Geoscience and Remote Sensing, 38, 1387–1398, https://doi.org/10.1109/36.843033, publisher: Institute of Electrical and Electronics Engineers (IEEE), 2000.

Massom, R. A., Eicken, H., Hass, C., Jeffries, M. O., Drinkwater, M. R., Sturm, M., Worby, A. P., Wu, X., Lytle, V. I., Ushio, S., Morris, K., Reid, P. A., Warren, S. G., and Allison, I.: Snow on Antarctic sea ice, Reviews of Geophysics, 39, 413–445, https://doi.org/10.1029/2000RG000085, 2001.

Mathew, N., Heygster, G., and Melsheimer, C.: Surface Emissivity of the Arctic Sea Ice at AMSR-E Frequencies, IEEE Transactions on Geoscience and Remote Sensing, 47, 4115–4124, https://doi.org/10.1109/TGRS.2009.2023667, 2009.

Matsumura, Y. and Ohshima, K. I.: Lagrangian modelling of frazil ice in the ocean, Annals of Glaciology, 56, 373–382, https://doi.org/10.3189/2015aog69a657, publisher: International Glaciological Society, 2015.

Meier, W. and Notz, D.: A note on the accuracy and reliability of satellite-derived passive microwave estimates of sea-ice extent, Clic Arctic sea ice working group, Consensus document, CLIC International Project Office, 2010.

Meier, W. N. and Stewart, J. S.: Assessment of the Stability of Passive Microwave Brightness Temperatures for NASA Team Sea Ice Concentration Retrievals, Remote Sensing, 12, 2197, https://doi.org/10.3390/rs12142197, 2020.

Meier, W. N. and Stroeve, J.: Comparison of sea-ice extent and ice-edge location estimates from passive microwave and enhanced-resolution scatterometer data, Annals of Glaciology, 48, 65–70, https://doi.org/10.3189/172756408784700743, 2008.

Meier, W. N., Markus, T., Comiso, J., Ivanoff, A., and Miller, J.: Sea ice algorithm theoretical basis document, 2017.

Meissner, T. and Wentz, F.: An updated analysis of the ocean surface wind direction signal in passive microwave brightness temperatures, IEEE Transactions on Geoscience and Remote Sensing, 40, 1230–1240, https://doi.org/10.1109/TGRS.2002.800231, 2002.

Meissner, T. and Wentz, F.: The complex dielectric constant of pure and sea water from microwave satellite observations, IEEE Transactions on Geoscience and Remote Sensing, 42, 1836 – 1849, 2004.

Monahan, E. and Lu, M.: Acoustically relevant bubble assemblages and their dependence on meteorological parameters, IEEE Journal of Oceanic Engineering, 15, 340–349, https://doi.org/10.1109/48.103530, 1990.

Morison, J. and McPhee, M.: Ice–ocean Interaction, in: Encyclopedia of Ocean Sciences, pp. 1271–1281, Elsevier, ISBN 978-0-12-227430-5, https://doi.org/10.1006/rwos.2001.0003, 2001.

Mätzler, C., ed.: Thermal Microwave Radiation: Applications for Remote Sensing, no. 52 in IET electromagnetic waves series, IET, London, ISBN 978-0-86341-573-9 978-1-84919-002-2, https://doi.org/10.1049/PBEW052E, 2006.

Nicolaus, M., Haas, C., and Willmes, S.: Evolution of first-year and second-year snow properties on sea ice in the Weddell Sea during spring-summer transition, Journal of Geophysical Research: Atmospheres, 114, 2008JD011 227, https://doi.org/10.1029/2008JD011227, 2009.

Notz, D. and Worster, M. G.: Desalination processes of sea ice revisited, Journal of Geophysical Research: Oceans, 114, 2008JC004 885, https://doi.org/10.1029/2008JC004885, 2009.

Parkinson, C. L. and Cavalieri, D. J.: Arctic sea ice variability and trends, 1979–2006, Journal of Geophysical Research: Oceans, 113, https://doi.org/10.1029/2007jc004558, publisher: American Geophysical Union (AGU), 2008.

Paul, F., Mielke, T., Schwarz, C., Schröder, J., Rampai, T., Skatulla, S., Audh, R. R., Hepworth, E., Vichi, M., and Lupascu, D. C.: Frazil Ice in the Antarctic Marginal Ice Zone, Journal of Marine Science and Engineering, 9, 647, https://doi.org/10.3390/jmse9060647, publisher: MDPI AG, 2021.

Petrich, C. and Eicken, H.: Overview of sea ice growth and properties, in: Sea Ice, edited by Thomas, D. N., pp. 1–41, Wiley, 1 edn., ISBN 978-1-118-77838-8 978-1-118-77837-1, https://doi.org/10.1002/9781118778371.ch1, 2017.

Picard, G., Royer, A., Arnaud, L., and Fily, M.: Influence of meter-scale wind-formed features on the variability of the microwave brightness temperature around Dome C in Antarctica, The Cryosphere, 8, 1105–1119, https://doi.org/10.5194/tc-8-1105-2014, 2014.

Picard, G., Sandells, M., and Löwe, H.: SMRT: an active–passive microwave radiative transfer model for snow with multiple microstructure and scattering formulations (v1.0), Geoscientific Model Development, 11, 2763–2788, https://doi.org/10.5194/gmd-11-2763-2018, 2018.

Picard, G., Löwe, H., Domine, F., Arnaud, L., Larue, F., Favier, V., Le Meur, E., Lefebvre, E., Savarino, J., and Royer, A.: The Microwave Snow Grain Size: A New Concept to Predict Satellite Observations Over Snow-Covered Regions, AGU Advances, 3, e2021AV000 630, https://doi.org/10.1029/2021AV000630, 2022.

Polder, D. and Van Santeen, J.: The effective permeability of mixtures of solids, Physica, 12, 257–271, https://doi.org/10.1016/S0031-8914(46)80066-1, 1946.

Purich, A. and Doddridge, E. W.: Record low Antarctic sea ice coverage indicates a new sea ice state, Communications Earth & Environment, 4, 314, https://doi.org/10.1038/s43247-023-00961-9, 2023.

Soriot, C., Picard, G., Prigent, C., Frappart, F., and Domine, F.: Year-round sea ice and snow characterization from combined passive and active microwave observations and radiative transfer modeling, Remote Sensing of Environment, 278, 113 061, https://doi.org/10.1016/j.rse.2022.113061, 2022.

Steffen, K. and Schweiger, A.: NASA team algorithm for sea ice concentration retrieval from Defense Meteorological Satellite Program special sensor microwave imager: Comparison with Landsat satellite imagery, Journal of Geophysical Research: Oceans, 96, 21 971–21 987, https://doi.org/10.1029/91JC02334, 1991.

Swift, C. T., Fedor, L. S., and Ramseier, R. O.: An algorithm to measure sea ice concentration with microwave radiometers, Journal of Geophysical Research: Oceans, 90, 1087–1099, https://doi.org/10.1029/jc090ic01p01087, publisher: American Geophysical Union (AGU), 1985.

Toyota, T., Massom, R., Tateyama, K., Tamura, T., and Fraser, A.: Properties of snow overlying the sea ice off East Antarctica in late winter, 2007, Deep Sea Research Part II: Topical Studies in Oceanography, 58, 1137–1148, https://doi.org/10.1016/j.dsr2.2010.12.002, 2011.

Tsang, L., Kong, J. A., and Shin, R. T.: Theory of microwave remote sensing, Wiley series in remote sensing, Wiley, New York, ISBN 978-0-471-88860-4, 1985.

Vichi, M.: An indicator of sea ice variability for the Antarctic marginal ice zone, The Cryosphere, 16, 4087–4106, https://doi.org/10.5194/tc-16-4087-2022, number: 10, 2022.

Wang, Z., Fraser, A. D., Reid, P., O'Farrell, S., and Coleman, R.: Antarctic sea ice surface temperature bias in atmospheric reanalyses induced by the combined effects of sea ice and clouds, Communications Earth & Environment, 5, 552, https://doi.org/10.1038/s43247-024-01692-1, 2024.

Willmes, S., Nicolaus, M., and Haas, C.: The microwave emissivity variability of snow covered first-year sea ice from late winter to early summer: a model study, The Cryosphere, 8, 891–904, https://doi.org/10.5194/tc-8-891-2014, 2014.

Worby, A.: Studies of the Antarctic sea ice edge and ice extent from satellite and ship observations, Remote Sensing of Environment, 92, 98–111, https://doi.org/10.1016/j.rse.2004.05.007, 2004a.

Worby, A.: Studies of the Antarctic sea ice edge and ice extent from satellite and ship observations, Remote Sensing of Environment, 92, 98–111, https://doi.org/10.1016/j.rse.2004.05.007, 2004b.

Yin, X., Boutin, J., Dinnat, E., Song, Q., and Martin, A.: Roughness and foam signature on SMOS-MIRAS brightness temperatures: A semi-theoretical approach, Remote Sensing of Environment, 180, 221–233, https://doi.org/10.1016/j.rse.2016.02.005, 2016.